Link to publisher version: *http://dx.doi.org/10.1016/j.oceaneng.2016.10.019*

Citation: Sui T, Zheng J, Zhang C et al (2017) Consolidation of unsaturated seabed around an inserted pile foundation and its effects on the wave-induced momentary liquefaction. Ocean Engineering. 131: 308-321.

Consolidation of unsaturated seabed around an inserted pile foundation and its effects on the wave-induced momentary liquefaction

Titi Sui [1,2], Jinhai Zheng [1,2], Chi Zhang [1,2*], Dong-Sheng Jeng [3], Jisheng Zhang [1,2], Yakun Guo [1,4*], Rui He [1,2]

[1] *State Key Laboratory of Hydrology-Water Resources and Hydraulic Engineering, Hohai University, Nanjing, China.*

[2] *College of Harbour, Coastal and Offshore Engineering, Hohai University, Nanjing, China.*

[3] *Griffith School of Engineering, Cities Research Centre, Griffith University Gold Coast Campus, Queensland, Australia.*

[4] *School of Engineering, University of Bradford, Bradford, BD7 1DP, UK.*

***Corresponding authors: zhangchi@hhu.edu.cn; y.guo16@bradford.ac.uk**

Highlights:

1. A 3D numerical model for evaluating the seabed shear failure instability around an inserted pile foundation due to its consolidation state was established.

2. Effects of the pile inserted depth, external loadings and seabed parameters on the surrounding seabed consolidation process were systematically investigated.

3. Effects of the initial seabed consolidation around an inserted pile on evaluating the wave-induced seabed momentary liquefaction were carefully examined.

Abstract: Seabed consolidation state is one of important factors for evaluating the foundation stability of the marine structures. Most previous studies focused on the seabed consolidation around breakwaters standing on the seabed surface. In this study, a numerical model, based on Biot's poro-elasticity theory, is developed to investigate the unsaturated seabed consolidation around a nearshore pile foundation, in which the pile inserted depth leads to a different stress distribution. Seabed instabilities of shear failure by the pile self-weight and the potential liquefaction under the dynamic wave loading are also examined. Results indicate that (1) the presence of the inserted pile foundation increases the effective stresses below the foundation, while increases and decreases the effective stresses around the pile foundation for small (de/R<=3.3) and large (de/R>3.3) inserted depths, respectively, after seabed consolidation, (2) the aforementioned effects are relatively more significant for small inserted depth, large external loading, and small Young's modulus, (3) the shear failure mainly occurs around the inserted pile foundation, rather than below the foundation as previously found for the located marine structures, and (4) wave-induced momentary liquefaction near the inserted pile foundation significantly increases with the increase of inserted depth, due to the change of seabed consolidation state.

Keywords: Seabed consolidation; pile foundation; external loading; wave; momentary liquefaction

1. Introduction

Seabed stability around marine structures is one of the main factors that must be considered in the foundation design. It has been well known that the seabed would suffer long-time consolidation under the gravity loading of the marine structures (Krost et al., 2011). This long-time consolidation may cause the complex stress distribution, the excess pore pressure dissipation and the seabed continuous subsidence (Ye, 2012b). Inappropriate design of the foundation may result in the shear failure of the surrounding soil and the structure collapse (Chung et al., 2006). Most of previous studies focused on the seabed liquefaction and scour under the dynamic wave and current loadings (Ye and Jeng, 2012; Sui et al., 2016; Sumer, 2014; Zhang et al., 2015; Zhou et al., 2015), but less attention was paid to the shear failure within the seabed during the consolidation process. Due to its practical importance for engineering construction, reliable and appropriate assessment of the seabed consolidation state is therefore required.

The classic Biot's poro-elasticity theory (Biot, 1956) has been commonly used to describe the relationship between the pore water flow and the deformation of soil skeleton, as well as to study the consolidation problems (Ferronato et al., 2010). Using a finite element model, Krost et al. (2011) simulated the seabed consolidation beneath the partially embedded pipeline. Ulker et al. (2010) considered the pre-consolidation of the unsaturated seabed in the investigation of the standing-wave induced seabed response. Ye (2012b) investigated the long-time seabed consolidation under the permeable composite breakwater, in which the effect of buoyancy force was considered. Jeng and Ye (2012) developed a 3D consolidation model, and discussed the distributions of seabed stresses and displacements under the rubble mound breakwater. Ye et al. (2012) further extended this model to deal with the seabed consolidation around an impervious rigid caisson breakwater, and used the consolidation state as the initial condition for simulating dynamic seabed response under 3D wave loading. Though these studies have demonstrated some features of the consolidation, they mainly focus on the seabed consolidation around the breakwaters which stand on the seabed.

The behavior of seabed consolidation around an inserted pile foundation is considerably different from that below a breakwater, since a part of the pile foundation is inserted into the seabed and this would cause a more complex seabed-structure interaction with a three-dimensional (3D) interface. The seabed stresses and displacements will be affected by the inserted depth of the pile. Some previous studies in this field focused on the pile behavior affected by the consolidated soil, which neglected the excess pore pressure dissipation, effective stresses and seabed subsidence during the consolidation process (Abdrabbo and Ali, 2015; Lee and Ng, 2004). There are a few analytical solutions for the seabed consolidation at the sides of the pile (Castro and Sagaseta, 2009; Lu et al., 2011; Randolph and Wroth, 1979). However, in these studies, the effects of the pile on its surrounding soil were simplified as the external loading or initial deformation at the soil-pile interface, which did not consider the gravity of the pile and could not fully represent the 3D soil-pile interactions. In addition, the aforementioned studies have not investigated the effects of saturation degree on the pore pressure dissipation during the seabed consolidation process around a pile foundation.

Since the effective stresses are strengthened around the structures because of the seabed consolidation, this will affect the soil liquefaction under the dynamic wave loading. Jeng et al. (2013) and Ye et al. (2014) considered effects of the seabed consolidation in simulating wave-induced seabed liquefaction around the composite breakwater. Zhao et al. (2014) studied the effects of initial seabed effective stresses on the liquefaction depth around a buried pipeline. It is found that the increased gravity of the pipeline would suppress the liquefaction in its vicinity. However, these studies focused on the marine structures that are located on the seabed and were limited to two-dimensional (2D) cases. When a pile is inserted into seabed, the effective stresses of its surrounding seabed would be significantly changed and exhibit a different distribution pattern compared to a located structure. The change of the overburden pressure would result in a different liquefaction zone under dynamic wave loading. Li et al. (2011) and Zhang et al. (2015) used 3D models to examine the wave-induced liquefaction zone around a pile foundation. However, effects of the seabed consolidation state around an inserted pile on wave-induced liquefaction have not been considered in previous studies.

In this study, a 3D numerical model is developed to systematically investigate the unsaturated seabed consolidation around an inserted pile foundation, in which the gravity of the pile is considered. The behavior of the seabed consolidation for various inserted depths of pile foundation, external loadings, soil permeability, saturation degree and Young's modulus is studied. The shear failure zone around the pile foundation is discussed. Finally, an analysis on the seabed liquefaction under a progressive wave is presented, in which effects of the seabed consolidation around an inserted pile are highlighted.

2. Numerical Model

2.1 Governing equations

In general, the grains or particles constituting the soil are more or less bound together by certain molecular forces and constitute a porous material with elastic properties, and the voids are filled with pore water. These concepts were first applied by Terzaghi (1925) in the analysis of the settlement of a soil column under a constant load. Based on this assumption, the elastic model for soil response under the dynamic wave loading was proposed by Biot (1956). Based on Biot's poro-elasticity theory, the governing equations which considers the acceleration of fluid and soil skeleton (FD model) could be expressed as (Zienkiewicz et al., 1980):

$$\sigma_{ij,j} + \rho g_i = \rho \ddot{u}_i + \rho_f \ddot{w}_i \tag{1}$$

$$-p_{,i} + \rho_f g_i = \rho_f \ddot{u}_i + \frac{\rho_f \ddot{w}_i}{n} + \frac{\rho_f g_i}{k_i} \dot{w}_i \tag{2}$$

$$\dot{u}_{i,i} + \dot{w}_{i,i} = -n\beta\dot{p} \tag{3}$$

where σ_{ij} is the total stress, ρ is the average density of the porous medium, p is the pore pressure, ρ_f is the density of water, g_i is the gravitational acceleration in the i-direction, u_i is the displacement of the soil matrix in the i-direction, w_i is the average relative displacement of the fluid to the solid skeleton in the i-direction, k_i is the permeability of the porous medium in the i-direction, n is the porosity of the solid phase. It should be noted that, ignoring the acceleration due to pore fluid or/and soil motion reduces these general formulations to the conventional "Partial-dynamic (PD)" or the "Quasi-dynamic (QS)" model. For seabed consolidation under the static gravity force of the pile, "QS" or "PD" model is sufficient for this process simulation. However, for wave-induced seabed dynamic response around the marine structure which allows slight displacements, the "FD" model is highly recommended to be used for obtaining a reliable numerical accuracy (Ulker et al., 2010). In this study, besides seabed consolidation process, the seabed liquefaction potential under dynamic wave loading around a pile is also discussed. Therefore, the fully-dynamic (FD) model is used here for the consistency of the governing equations in the present study.

The equivalent compressibility of pore water and entrapped air β is defined as

(Yamamoto et al., 1978):

$$\beta = \frac{1}{k_w} + \frac{1 - S_r}{\rho_f g d} \tag{4}$$

where d is the water depth, S_r is the saturation degree, k_w is the bulk modulus of the pure water which is taken as 1.95×10^{9} N/m^2. This expression takes the saturation degree into account in the deformation of the porous medium. It is noted that this definition is only valid for a high saturation degree (e.g. $S_r > 0.95$) (Pietruszczak and Pande, 1996).

The total stresses can be expressed in terms of the effective stresses (σ_{ij}) and pore pressure (p):

$$\sigma_{ij} = \sigma'_{ij} - \delta_{ij} p \tag{5}$$

The effective stress-strain relation can be written as:

$$\sigma'_{i,j} = \lambda \varepsilon_{kk} \delta_{ij} + 2G\varepsilon_{ij} \tag{6}$$

$$\varepsilon_{ij} = \frac{u_{i,j} + u_{j,i}}{2} \tag{7}$$

where δ_{ij} is the Kronecker delta denotation, σ'_{ij} is the effective stress, ε_{ij} is the soil strain, λ=2$G\mu$(1-2μ), G is the shear modulus, μ is Poisson's radio. Note that the above definition implies a positive tensional stress.

2.2 Boundary conditions

Fig. 1 shows the (a) 3D Sketch and (b) appropriate boundary conditions of the present model. Three elements of water, seabed and pile are considered in the current model. The inserted pile is presented at the center of the computational domain. The lateral and bottom boundaries of the seabed are considered as impermeable and rigid, where the displacements of the seabed and the normal gradient of pore pressure are zero ($u_{soil}=0$, $\partial p/\partial n=0$ (n is the unit normal on the boundaries)). Pore pressure at the seabed surface is equal to the water pressure ($p_b=\rho_f gd$). The normal stress and shear stress vanish at the seabed surface. At the top of the pile foundation, an external loading P_v in the vertical direction is applied, which represents the weight of the upper structures (*e.g.*, sea-crossing bridge, oil platform and wind turbines).

Unlike the most previous studies, which solve the response of the seabed/structure as a whole system, the present model includes an internal boundary condition at the soil-pile interface. Specifically, the normal gradient of pore pressure is set to zero ($\partial p/\partial n=0$), representing the rigid and impermeable surface of the pile. In addition, the soil displacement is equal to the pile displacement ($u_{soil}=u_{pile}$) ("no-slip" boundary condition), and the total stress equilibrium is maintained ($\sigma'_{pile}=\sigma'_{soil}-p,\ \tau_{pile}=\tau_{soil}$) at the soil-pile interface. It should be noted that, this "no-slip" assumption was usually adopted in the poro-elastic models when the minimal deformation happens with soil and structure, for the first-hand simplification (Jeng et al., 2013; Ye et al., 2014). In this study, the maximum subsidence of the seabed during the consolidation process is less than one centimeter (1 ‰ of the pile length, seen in Fig. 10), which validates the reasonable usage of this assumption.

3. Model validation

While the present model has been validated for wave-induced dynamic seabed response in Sui et al. (2016) and Zhang et al. (2015), it is further validated for seabed consolidation in this study for the completeness and convenience. The model is first validated by the one-dimensional (1D) Terzaghi's consolidation theory (Terzaghi, 1925). As shown in Fig. 2a, a constant loading is imposed on the seabed surface where only the drainage is allowed. Based on the Terzaghi's consolidation theory, Wang (2000) provided a set of analytical solutions for the seabed displacements and pore pressure during the consolidation process. In the present case, parameters simulated are: the vertical loading P=10 kPa, the seabed permeability k=1.0×10^{-5} m/s, the elasticity modulus E=100 MPa, the Poisson's ratio μ=0.25, saturation degree S_r=1, porosity n=0.3, and density ρ_s=2650 kg/m^3. Fig. 2b and Fig. 2d show the vertical distributions of the pore pressure and the vertical soil displacement at various times indicated (t=60s, 600s, 1500s and 3000s). Fig. 2c illustrates the temporal varying subsidence of the soil particles at the seabed surface. Very good agreements are obtained between the numerical model and the analytical solution. It shows that, as time goes, the resistance force to the external loading is transferred from the pore water to the soil skeletons, leading to the compression of the soil skeleton in the vertical direction.

Ye et al. (2012) used a finite element model (ADINA-SWANDYNE II, Chan (1988)) to simulate the unsaturated seabed consolidation and shear failure beneath a 3D rigid caisson breakwater. The gravity loading from structure were considered (see Fig. 3a). Fig. 3(b-d) presents the comparison of the seabed variables (the pore pressure, the effective stress and the vertical settlement) obtained using the present model and by Ye et al. (2012). In the present case, parameters simulated are: the seabed permeability k=1.0×10^{-5} m/s, the elasticity modulus E=20 MPa, the Poisson's ratio μ=0.33, saturation degree S_r=0.98, porosity n=0.25, and density of soil and structure $\rho_s(\rho_{str})$=2650 kg/m^3. It is seen that all variables rapidly change at the beginning of the consolidation, and reach a relatively stable state after about 20,000s. The present model well reproduces the results of Ye et al. (2012) with regard to both the magnitudes and the variation patterns of the seabed variables.

4. Seabed consolidation around the pile foundation

In this section, the present model is applied to simulate the seabed consolidation process around the pile foundation. The distributions of seabed effective stresses and pore pressures are firstly given around the pile foundation without considering the external loading. The effects of the external loading P_v on the pore pressure, the effective stress and seabed subsidence are then discussed. Finally, the shear failure of the seabed around the pile is examined to provide reference for engineering practice. Table 1 lists the parameters of the seabed and pile simulated. It should be noted that, due to the various types of mono-pile in the practical engineering case, this study does not assign one specific material to the pile. The density value (2650 kg/m^3) used in the study corresponds to the materials, such as stone or concrete and only for the purpose of demonstration. Numerical tests indicate that the soil effective stresses and displacements around the pile are not affected by the lateral boundary if their distance exceeds 25R (R is the radius of the pile). In this study, the lateral boundary is set as 30R away from the pile so that the lateral boundary effects can be ignored. The details of the model setup is shown in Fig. 1b.

The seabed consolidation may take a long time to reach its final state, due to the gradual dissipation of the excess pore pressure and compression of the soil skeleton. This duration may be a few minutes for the coarse soil or a few years for the clay with an extremely low permeability. Based on the 1D Terzaghi's consolidation theory, the time for completing the 90% consolidation could be expressed as (Wang, 2000):

$$t_{90} = T_v \frac{d^2}{C_v} \tag{8}$$

$$C_v = \frac{2Gk(1-\mu)}{\gamma_w(1-2\mu)} \tag{9}$$

where, T_v=0.848 is the vertical consolidation time factor for the 90% consolidation, C_v is the consolidation coefficient, $\gamma_w=\rho_f g$ is the bulk specific weight of the pore water. According to Eq. (8), the longest time for reaching the 90% consolidation state in the computational cases of this section is estimated as 6,800s. Therefore, we set the computational time in the model as 40,000s for all the cases presented below, ensuring that the whole consolidation has been finished for all cases.

4.1 Distributions of the effective stresses and pore pressure

Fig. 4 shows the distributions of the pore pressure, the effective stresses and the vertical displacements after consolidation with and without the pile foundation. It is shown that the distribution of the pore pressure is the same with (Fig. 4, right column) and without (Fig. 4, left column) a pile foundation. However, the presence of the pile foundation remarkably increases the effective stress of the underneath soil (Fig. 4c and Fig. 4d). This is because after the long-time consolidation, the pile gravity is totally supported by the soil skeleton. It is found that the concentration zone of the effective stress locates just below the pile foundation. This may be attributed to the sharp change of Young’s modulus between seabed and pile at their interface. Simulation also shows the phenomenon of stress concentration within the pile due to the stress equilibrium boundary condition (section 2.2) at the seabed-pile interface, and this further validates the phenomenon of stress concentration within seabed at the pile corner. The seabed around the pile foundation subjects to a larger amount of subsidence due to the additional pile gravity (Fig. 4e and Fig. 4f).

Fig. 5 shows the distributions of the horizontal soil displacements and the effective normal stresses around the pile foundation in the *x*-*y* plane. Comparing with the displacement (u_z) and stress (σ'_z) in the vertical direction (Fig. 4), all the horizontal variables (u_x, u_y, σ'_x and σ'_y) are much smaller. This may be ascribed to the fact that the generations of u_x (u_y) and σ'_x (σ'_y) are due to the small horizontal compression of the soil skeleton, which is an indirect deformation caused by the non-uniform vertical subsidence around the pile (Fig. 4f). Fig. 5a illustrates that u_x is positive-negative symmetric with *x*-axis (x=0) and has the largest value in the vicinity of the pile. This is due to the fact that the pile/seabed subsidence will cause the surrounding soil moving towards to the center. Such movement causes an interesting distribution pattern of σ'_x, which varies around the value of -0.218$\gamma_w d$ (σ'_{x0}, the value of σ'_x without pile) in the vicinity of the pile foundation (Fig. 5c). Negative $\Delta\sigma'_x$ (σ'_x - σ'_{x0}) is mainly found at the sides and the vicinity of the pile which is symmetric with y=0, indicating seabed in this domain is relatively compressed in the *x* direction when a pile is presented. Correspondingly, seabed at the head and rear of the pile is relatively tensioned with a positive value of $\Delta\sigma'_x$. Similar phenomenon of u_y and σ'_y can be found in Fig. 5(b) and Fig. 5(d), except that they behave the symmetric distribution with *y*-axis (y=0).

4.2 Effects of the inserted depth (d_e)

The effect of the inserted depth of the pile foundation on the nearby seabed consolidation is one of the main objectives of this study, since most of the previous studies only considered the structures standing on the seabed surface (i.e., de/R=0). Fig. 6 shows the change of the seabed stresses due to the inserted pile foundation. It is found that both the vertical effective normal stress and the shear stress are significantly changed in the vicinity of the pile, and decrease with the increase of the pile inserted depth. This can be ascribed to the fact that when the pile foundation is inserted into the seabed, the buoyancy force acting on the bottom of the pile foundation increases, thus reducing the loads imposing on the nearby soil skeleton.

Fig. 7 illustrates the vertical distribution of the vertical effective normal stresses (σ'_z) for various inserted depths. Results are shown at two locations (S_1 and S_2) in front of and below the pile foundation. $\Delta\sigma'_z=\sigma'_{z(without\ pile)}-\sigma'_{z(with\ pile)}$ denotes the difference in the effective stresses due to the inserted pile foundation, which represents the significance of the inserted pile foundation. In front of the pile foundation (S_1 location), σ'_z decreases as the inserted depth increases. For smaller inserted depth, a large positive $\Delta\sigma'_z$ is found. For larger inserted depth (i.e. de/R>3.3), however, $\Delta\sigma'_z$ could decrease to be negative. This is because the compression of the surrounding soil is greatly decreased due to the "no-slip" boundary at the soil-pile interface. Below the pile foundation (S_2 location), σ'_z is large for the located foundation (de/R=0) and owns a relative small value for the inserted foundation (de/R>0). When the pile is inserted into the seabed, σ'_z increases as the inserted depth increases which is because the decreasing compression of the soil at the lateral sides (as discussed above) decreases its supports to the pile. However, $\Delta\sigma'_z$ at the bottom of the pile foundation seems to decrease with the increasing inserted depth, indicating that the influence of the inserted pile foundation becomes relatively smaller if the inserted depth is large.

In Fig. 8, the maximum amplitudes $\Delta\sigma'_{z,max}$ are used at both locations (S_1 and S_2) to demonstrate how the significance of the inserted pile foundation changes for various seabed parameters (permeability, saturation degree and Young's modulus). It is found that (1) increasing the seabed permeability and saturation degree has little influence on $\Delta\sigma'_{z,max}$, and (2) the increasing Young's modulus leads to the decrease of $\Delta\sigma'_{z,max}$. This indicates that the significance of the inserted pile foundation on the effective stresses is more pronounced for smaller Young's modulus. The reason is that the soil skeleton suffers more deformation with a low Young's modulus, leading to a more obvious change of the effective stresses in the vicinity of the pile foundation.

4.3 Effects of the external loading

In this section, using the aforementioned consolidation state as the initial condition, an external loading is imposed on the top of the pile. This will take time for the seabed to achieve a new consolidation state. Fig. 9 illustrates the pore pressure distribution (color) and the seepage flow (arrows) around the pile foundation at t=300 s (Fig. 9a) and t=3,000 s (Fig. 9b) after imposing the external loading. When the new consolidation is not completed (t=300 s), the pore pressure is concentrated below the pile foundation which leads to the outward drainage of the pore water. After the new consolidation is completed (t=3,000 s), the excess pore pressure has been fully dissipated and the seepage flow no longer exists. Fig. 10 plots the temporal variation of the seabed variables below the pile foundation. It is found that the pore pressure (the effective stress) increases (decreases) to its peak within a short time, then gradually decreases (increases) towards to a stable value (see Fig. 10a and 10b). This indicates that the resistance force to the external loading is transferred from the pore water to the soil skeleton during this process. It is also found that the drainage of the pore water leads to further compression of the soil skeleton, as well as the further settlement of the pile (see Fig. 10c).

Fig. 11 and Fig. 12 illustrate the effects of the seabed permeability and degree of saturation (S_r=1.0 means the saturated seabed) on the dissipation of the excess pore pressure below the pile foundation, respectively. It is seen that the peak of the pore pressure at the beginning of consolidation is higher for lower permeability and greater saturation degree. On the other hand, the dissipation of the excess pore pressure is slower for lower permeability and lower saturation degree, since lower values of these two parameters will impede the drainage of pore water.

Fig. 13 shows the distribution of the effective stress σ'_z under various external loadings after seabed consolidation. It is seen that the effective stress σ'_z within the pile foundation and its surrounding seabed increases with the increase of the external loading. Not only around the pile corner, the concentration of σ'_z is also found at the seabed surface which is adjacent to the pile. Fig. 13 also shows the phenomenon of stress concentration is more strengthened under the larger external loadings.

4.4 Shear failure

Shear failure is one type of seabed instability (Rahman, 1997; Jeng, 2012; Sumer, 2014), which may happen when the shear stresses at a point within the marine sediment is significantly large to overcome its shear failure resistance. This type of seabed instability is mostly induced by the gravity force and storms, which may cause a horizontal movement (or slides) of the sediment (Jeng, 2012). In this section, based on the Mohr-Column criterion, the shear failure instability of seabed under the gravity force of the pile is examined to improve the pile's protection strategy before its construction. The shear failure zone within seabed around the inserted pile foundation is simulated. Effects of the external loading and inserted depth on the shear failure zone are also examined.

Based on the Mohr-Coulomb criterion, shear failure at a given point occurs if the stress angle φ' is greater than the friction angle φ'_f (Fig. 14). This criterion is expressed as (Armenàkas, 2005)

$$\varphi' = \arcsin\left(\frac{\dfrac{\sigma'_1 - \sigma'_3}{2}}{\dfrac{c}{\tan\varphi'_f} + \dfrac{\sigma'_1 + \sigma'_3}{2}}\right) \geq \varphi'_f \tag{10}$$

$$\begin{aligned}
\sigma'_1 &= \frac{I_1}{3} + \frac{2}{3}\left(\sqrt{I_1^2 - 3I_2}\right)\cos\alpha \\
\sigma'_2 &= \frac{I_1}{3} + \frac{2}{3}\left(\sqrt{I_1^2 - 3I_2}\right)\cos\left(\alpha + \frac{2\pi}{3}\right) \\
\sigma'_3 &= \frac{I_1}{3} + \frac{2}{3}\left(\sqrt{I_1^2 - 3I_2}\right)\cos\left(\alpha + \frac{4\pi}{3}\right)
\end{aligned} \tag{11}$$

$$\begin{aligned}
\alpha &= \frac{1}{3}\cos^{-1}\left(\frac{2I_1^3 - 9I_1I_2 + 27I_3}{2\left(I_1^2 - 3I_2\right)^{3/2}}\right) \\
I_1 &= \sigma'_x + \sigma'_y + \sigma'_z \\
I_2 &= \sigma'_x\sigma'_y + \sigma'_y\sigma'_z + \sigma'_z\sigma'_x - \tau_{xy}^2 - \tau_{yz}^2 - \tau_{xz}^2 \\
I_3 &= \sigma'_x\sigma'_y\sigma'_z - \sigma'_x\tau_{yz}^2 - \sigma'_y\tau_{xz}^2 - \sigma'_z\tau_{xy}^2 + 2\tau_{xy}\tau_{yz}\tau_{xz}
\end{aligned} \tag{12}$$

where c' and φ'_f are the cohesion and friction angle of the sand soil, respectively, σ'_1, σ'_2 and σ'_3 are the maximum, intermediate and minimum principal effective stresses, respectively. The friction angle φ'_f of sand soil generally varies from 30° to 45°, and is set to 40° in the present study.

Fig. 15 illustrates the distributions of the stress angle φ' and the shear failure zone around the pile foundation after the seabed consolidation. Unlike the results of Ye et al. (2012) which showed the larger φ' existing below the located breakwater, the present study reveals that φ' is relatively small below the inserted pile foundation but is large at the lateral sides and surface (see Fig. 15a). This is because the inserted pile foundation changes the distributions of both the normal and shear stresses within the seabed. In this case, the soil skeleton at the lateral sides is more tensioned. Therefore, shear failure mainly happens at the lateral sides of the inserted pile foundation (see Fig. 15b). This phenomenon is only presented with an inserted structure foundation. It is seen that no shear failure occurs in the seabed in the vicinity of the pile foundation (see Fig. 15b). This is because the “no-slip” boundary condition at the soil-pile interface results in a relatively small shear stress angle there (see Fig. 15a).

Fig. 16 illustrates the shear failure zone around the pile foundation for various external loadings. The shear failure area increases as the external loading increases. It is noted that the shear failure zone close to the pile foundation is more sensitive to the change of the external loading, implying that this region is most unstable with respect to the shear failure destruction under a large external loading.

Fig. 17 illustrates the effects of the inserted depth on the shear failure zone around the pile foundation after the seabed consolidation. It is found that the seabed just below the pile foundation does not suffer shear failure, which behaves like a rigid object. This phenomenon has been presented in Ye et al. (2012) for the located marine structure (i.e., de/R=0), and is further extended for the inserted pile foundation in this study. As the inserted depth increases, the shear failure zone moves from the region below the foundation to the lateral sides of the foundation. This finding demonstrates that the shear failure is more likely to occur at the lateral sides of the inserted pile foundation rather than beneath it.

4.5 Effects of the seabed consolidation around the pile on the wave-induced momentary liquefaction

Generally speaking, based on the different ways that generate the excessive pore pressure (difference between the wave pressure and pore pressure), two mechanisms that named “residual liquefaction” and “momentary liquefaction” for wave induced soil liquefaction instability have been found and proposed by the previous investigations (Zen and Yamazaki, 1990; Sumer, 2014; Jeng, 2012). The residual liquefaction normally occurs as the consequence of the plastic deformation of soil skeleton and the excessive pore pressure is mainly caused by the pore pressure build-up (Sumer, 2014). On the other hand, the momentary liquefaction is due to the sharp upward pressure gradient induced by the momentary wave through, in which the phenomenon of pressure build-up does not dominant the whole process. When a wave propagates over the seabed floor, this upward pressure gradient would naturally generate the excessive pore pressure. If the excessive pore pressure exceeds overburden pressure, the vertical effective stresses of soil skeleton will decrease to zero and the momentary liquefaction happens (Jeng, 2012; Sumer, 2014). In general, momentary liquefaction most probably occurs in the unsaturated seabed with the relatively poor drainage condition (Zen et al., 1998). When reaching liquefaction state, the soil will behave like a liquid with no bearing capacity, affecting the stability of the pile foundation. In this study, the second mechanism of “momentary liquefaction” is only considered in evaluation of the seabed liquefaction instability around a near-shore pile foundation.

Zen and Yamazaki (1990) proposed the following 1D liquefaction criteria:

$$-(\gamma_s - \gamma_w)z \le p_0 - p_{b0} \tag{13}$$

where, p_0 is the wave-induced pore pressure, p_{b0} is the dynamic wave pressure on the seabed surface, γ_s and γ_w are the bulk specific weight of soil (not the grains) and water, respectively.

Jeng (1997) extended this criterion to 3D situation by adopting the average of the effective stresses:

$$-(\gamma_s - \gamma_w)\frac{1+2k_0}{3}z \le p_0 - p_{b0} \tag{14}$$

Where k_0 is the lateral compression coefficient of soil.

The above criteria are only suitable for the cases without the presence of marine structures. When marine structures are present, the surrounding soil will subject to further compression because of the additional gravity. The increased overburden pressure will suppress the liquefaction closed to the marine structures (Jeng et al., 2013; Ye et al., 2014; Zhao et al. 2014). Ye (2012a) compared several liquefaction criteria as commonly used in the past decades. For the liquefaction calculation around marine structures while considering the seabed consolidation, they recommended a modified criteria based on Zen and Yamazaki (1990) form, expressed as

$$\sigma'_{z0} \leq p_0 - p_{b0} \tag{15}$$

where σ'_{z0} is the initial vertical effective stress, which comes from the seabed consolidation. Previous studies focused on the seabed response and liquefaction around the pile under dynamic wave loading, but neglected the seabed consolidation under the long-time static loading of pile (Li et al., 2011; Sui et al., 2016; Zhang et al., 2015). As discussed in Section 4, the distribution of the effective stresses is remarkably changed by the presence of the pile. The initial effective stress may have little effect on the dynamic seabed response, but would significantly change the overburden pressure and affect the seabed liquefaction.

In this section, the initial consolidation state was considered in the evaluation of the seabed liquefaction around an inserted pile foundation, using Eq. (15). The dynamic wave pressure (P_{b0}) at the seabed surface needs to be specified as the boundary condition of the present model. As a preliminary examination, P_{b0} is provided by linear wave theory:

$$p_{b0} = \frac{\rho_f gH}{2\cosh(\lambda d)} e^{i(\lambda x - \omega t)} \tag{16}$$

where H is wave height, λ is wave number (determined by linear wave dispersion relation), ω is wave frequency. The parameters for wave, soil and pile simulated in numerical examples are: wave period T=8 s, wave height H=3 m, water depth d=8m, soil permeability $k=1\times10^{-4}$ m/s, soil shear modulus $E_s=1.6\times10^8$ pa, seabed saturation S_r=0.985, pile length l=24 m, pile inserted depth de=12 m and the vertical loading P_v=0 kPa. Other parameters can be found in Table 1.

Fig. 18 illustrates the (a-b) distribution of the pore pressure and (c-d) liquefaction zone under a progressive wave loading at t=3/8T and t=5/8T, respectively. The seepage force, which depends on the pore pressure gradient ($j_x=\partial p/\partial x$, $j_y=\partial p/\partial y$, $j_z=\partial p/\partial z$), was also considered in the simulation (arrows in Fig. 18). When the seepage force is upward, the pore water is forced to move upward which promotes the seabed to liquefy. On the contrary, when the seepage force is downward, liquefaction is unlikely to take place. This mechanism is clearly shown in Fig. 18. When the wave through reaches the front of the pile at t=3/8T, the wave-induced negative pore pressure p_0 and large value of the upward seepage force is found beneath the seabed (see Fig. 18a). This corresponds to the liquefaction zone around the pile which exhibits a 3D pattern (see Fig. 18c). The liquefaction depth L_d at the head is larger than that at the rear of the pile foundation, but smaller than that with a distance to the pile. This is because the presence of the pile increases the overburden pressure within its surrounding seabed. It is also interesting to find that the largest seepage force at the head of the pile (x=-1.5m, Fig. 18a) does not lead to the largest liquefaction depth there (the largest liquefaction depth occurs at x=-12m in

Fig. 18c). This is because the liquefaction potential is determined by the integration of the seepage force from a given location to the seabed surface, rather than by its largest value. It is also found that the seabed region under wave crest does not suffer liquefaction, where the downward seepage force dominates. At t=5/8T, similar phenomenon can be seen in Fig. 18b and Fig. 18d, in which the largest liquefaction depth occurs at the rear of the pile (x=2m).

The previous studies usually did not consider the seabed initial consolidation state under the structure gravity force when evaluating the liquefaction potential around a near shore pile (Li et al., 2011; Chang and Jeng, 2014). In their studies, the overburden pressure of soil was mostly assumed as $\sigma'_{z0}=-(\gamma_s-\gamma_w)z$ which may be underestimated in the vicinity of the pile. Fig. 19 illustrates the effects of the seabed initial consolidation states on the wave induced soil liquefaction zone. Numerical results indicate that the liquefaction depth around the pile decreases significantly if the seabed initial consolidation states is considered. This is because the initial consolidation state under the pile gravity force promotes a further compression of the soil skeleton, which naturally suppresses the seabed liquefaction under the dynamic wave loading.

Fig. 20 illustrates the maximum liquefaction zone around a pile foundation for various inserted depths. First, the presence of the pile foundation decreases the liquefaction depth near the pile. This is because the gravity of the pile enhances the compression of soil skeleton. Similar findings are obtained in Jeng et al. (2013) and Ye et al. (2014) who dealt with the located breakwater. However, this study additionally shows that compared to the situation of a located pile foundation (i.e., *de/R*=0), when the inserted depth of the pile foundation increases, the liquefaction depth within its surrounding seabed significantly increases. This is due to the decrease in the initial effective stress at the lateral sides of the pile foundation (see the discussions in Section 4).

5 Conclusion

A numerical model based on the Biot's equations is used to systematically investigate the unsaturated seabed consolidation around an inserted pile foundation. Both the dead loadings from the pile are considered. The model has been validated using the previous analytical solutions and numerical results for cases without a pile or the pile doesn't insert the seabed soil. Effects of the inserted depth and the external loading on the seabed consolidation process are then investigated for a range of seabed parameters using the validated model. Effects of the seabed consolidation around an inserted pile on the wave-induced liquefaction are also examined. The shear failure zone around the pile foundation is discussed. The main conclusions are drawn as following:

(1) The presence of the inserted pile foundation generates different behavior of the seabed consolidation. It increases the effective stresses below the foundation, while it

respectively increases (for smaller inserted depth, *de/R*<=3.3 m) and decreases (for larger inserted depth, *de/R*>3.3 m) the effective stresses around the pile foundation, after the seabed is consolidated.

(2) The additional external loading increases the effective normal stresses around the pile foundation. Greater permeability and degree of saturation lead to the quicker dissipation of the excessive pore pressure near the inserted pile foundation. Therefore, lesser time is needed to achieve a new consolidation state. The above effects are relatively more significant for smaller inserted depth, larger external loading, and smaller Young's modulus.

(3) The shear failure mainly occurs around the inserted pile foundation, rather than below the foundation as previously found for the located marine structures without an inserted foundation (e.g., breakwaters (Ye et al., 2012)).

(4) The consideration of the seabed initial consolidation states under the pile gravity force would decrease the wave-induced liquefaction depth around the pile foundation.

(5) Wave-induced liquefaction depth near the pile foundation significantly increases with the increase of the inserted depth, primarily due to the change of the seabed consolidation state.

The focus of this study is to investigate the seabed consolidation process by pile gravity and the shear failure instability, namely the authors investigate the pile which has already been installed in the seabed. The driving practice is neglected which is due to the limitation of the present model. Actually, the additional compactions and strengthening induced by pile driving is much complex (Hansen 2012), and its effects on the seabed stresses (displacements) distribution pattern would be further investigated in our next work.

Acknowledgements

This work is financially supported by the National Natural Science Foundation for Distinguished Young Scholars (51425901), the National Natural Science Foundation of China (51209082, 51209083), the Natural Science Foundation of Jiangsu Province (BK20161509), the Fundamental Research Funds for the Central Universities (2015B15514), Jiangsu Graduate Research and Innovation Plan Grant (#CXLX11_0450) and the 111 project (B12032). The comments and suggestions from reviewers have significantly improved the quality of the final manuscript.

References

Abdrabbo, F.M., Ali, N.A., 2015. Behaviour of single pile in consolidating soil. Alexandria Eng. J. 54(3), 481-495.

Armenàkas, A.E., 2005. Advanced mechanics of materials and applied elasticity, fifth Ed.

Prentice Hall, New Jersey.

Biot, M.A., 1956. Theory of propagation of elastic waves in a fluid-saturated porous solid. I. Low-frequency range. J. Acoust. Soc. Am. 28(2), 168-178.

Castro, J., Sagaseta, C., 2009. Consolidation around stone columns. Influence of column deformation. Int. J Numer. Anal. Met. 33(7), 851-877.

Chung, S., Kim, S., Kang, Y., Im, J., Prasad, K.N., 2006. Failure of a breakwater founded on a thick normally consolidated clay layer. Géotechnique 56(6), 393-409.

Chan A.H.C., 1988. A unified finite element solution to static and dynamic problems of geomechanics. PhD thesis, University of Wales, Swansea Wales.

Chang, K.T., Jeng, D.S. 2014. Numerical study for wave-induced seabed response around offshore wind turbine foundation in Donhai offshore winbed farm, Shanghai, China. Ocean Eng. 85: 32-43.

Ferronato, M., Castelletto, N., Gambolati, G., 2010. A fully coupled 3-D mixed finite element model of Biot consolidation. J. Comput. Phys. 229(12), 4813-4830.

Hansen NM., 2012. Interactions between seabed soil and offshore wind turbine foundations. PhD thesis, Technical University of Denmark, Copenhagen.

Jeng, D.S., 2012. Porous models for wave-seabed interactions. Springer, Berlin.

Jeng, D.S., Ye, J.H., 2012. Three-dimensional consolidation of a porous unsaturated seabed under rubble mound breakwater. Ocean Eng. 53, 48-59.

Jeng, D.S., 1997. Wave-induced seabed instability in front of a breakwater. Ocean Eng. 24(10), 887-917.

Jeng, D.S., Ye, J.H., Zhang, J.S., Liu, P.L.F., 2013. An integrated model for the wave-induced seabed response around marine structures: Model verifications and applications. Coast. Eng. 72, 1-19.

Krost, K., Gourvenec, S., White, D., 2011. Consolidation around partially embedded seabed pipelines. Geotechnique 61(2), 167-173.

Lee, C., Ng, C.W., 2004. Development of downdrag on piles and pile groups in consolidating soil. J. Geotech. Geoenviron. 130(9), 905-914.

Li, X.J., Gao, F.P., Yang, B., 2011. Wave-induced Pore Pressure Responses and Soil Liquefaction Around Pile Foundation. Int. J. Offshore Polar 21(3), 233-239.

Lu, M., Xie, K., Wang, S., Li, C., 2011. Analytical solution for the consolidation of a composite foundation reinforced by an impervious column with an arbitrary stress increment. Int. J. Geomech. 13(1), 33-40.

Pietruszczak, S., Pande, G., 1996. Constitutive relations for partially saturated soils containing gas inclusions. J. Geotech. Eng-ASCE 122(1), 50-59.

Rahman, M.S. 1997. Instability and movement of oceanfloor sediments: A review. Int. J. Offshore Polar Eng. 7(3), 220-225.

Randolph, M.F., Wroth, C., 1979. An analytical solution for the consolidation around a driven pile. Int. J. Numer. Anal. Met. 3(3), 217-229.

Sui, T., Zhang, C., Guo, Y., Zheng, J., Jeng, D.S., Zhang, J., Zhang, W., 2016. Three-dimensional numerical model for wave-induced seabed response around mono-pile. Ships Offshore Struc. 11 (6), 667-678.

Sumer, B.M., 2014. Liquefaction Around Marine Structures. World Scientific Publishing, Singapore.

Terzaghi K. 1925. Erdbaumechanik auf Bodenphysikalischer Grundlage. Vienna: F. Duticke.

Ulker, M., Rahman, M., Guddati, M., 2010. Wave-induced dynamic response and instability of seabed around caisson breakwater. Ocean Eng. 37(17), 1522-1545.

Wang, H.M., 2000. Theory of Linear Poroelasticity with Applications to Geomechanics and Hydrogeology. Princeton University Press, Princeton.

Yamamoto, T., Koning, H.L., Sellmeijer, H., Hijum, E.V., 1978. On the response of a poro-elastic bed to water waves. J Fluid Mech. 87(1), 193-206.

Ye, J.H., 2012a. 3D liquefaction criteria for seabed considering the cohesion and friction of soil. Appl. Ocean Res. 37, 111-119.

Ye, J.H., 2012b. Numerical modelling of consolidation of 2-D porous unsaturated seabed under a composite breakwater. Mechanics 18(4), 373-379.

Ye, J.H., Jeng, D.S., Chan, A.H.C., 2012. Consolidation and dynamics of 3D unsaturated porous seabed under rigid caisson breakwater loaded by hydrostatic pressure and wave. Sci. China Technol. Sc. 55(8), 2362-2376.

Ye, J.H., Jeng, D.S., 2012. Response of porous seabed to nature loadings: waves and currents. J. Eng. Mech.-ASCE. 138(6): 601-613.

Ye, J.H., Jeng, D.S., Liu, P.L.F., Chan, A.H.C., Wang, R., Zhu, C., 2014. Breaking wave-induced response of composite breakwater and liquefaction in seabed foundation. Coast. Eng. 85, 72-86.

Zen, K., Yamazaki, H., 1990. Oscillatory pore pressure and liquefaction in seabed induced by ocean waves. Soil Found. 30(4), 147-161.

Zen, K, Jeng, D.S., Hsu, J.R.C., Ohyama, T., 1998. Wave-induced seabed instability: difference between liquefaction and shear failure. Soils Found., 38(2), 37-47.

Zhang, C., Zhang, Q., Wu, Z., Zhang, J., Sui, T., Wen, Y., 2015. Numerical Study on Effects of the Embedded Monopile Foundation on Local Wave-Induced Porous Seabed Response. Math. Probl. Eng. 501, 184621.

Zhao, H.Y., Jeng, D.S., Guo, Z., Zhang, J.S., 2014. Two-dimensional model for pore pressure accumulations in the vicinity of a buried pipeline. J Offshore Mech. Arct. 136, 042001.

Zhou, X.L., Zhang, J., Guo, J.J., Wang, J.H., Jeng, D.S., 2015. Cnoidal wave induced seabed response around a buried pipeline. Ocean Eng. 101, 118-130.

Zienkiewicz, O., Chang, C., Bettess, P., 1980. Drained, undrained, consolidating and dynamic behaviour assumptions in soils. Geotechnique 30 (4), 385-395.

Table lists:

Table 1. Parameters used in the case studies

Figure lists:

Fig. 1. (a) 3D Sketch and (b) boundary conditions of the present model in which *d* is the water depth, *de* is the inserted depth of the pile foundation, *R* is the pile radius.

Fig. 2. Comparison of the seabed consolidation process using the numerical model (lines) and Terzaghi's consolidation theory (circles).

Fig. 3. Comparison of the pore pressure, effective stresses and vertical settlement at the location of 1m below the breakwater between the present model (lines) and Ye et al. (2012) (circles).

Fig. 4. Distributions of the pore pressure, vertical effective stresses and vertical displacements without (de/R=0, in the left column) and with (de/R=4.7, in the right column) the pile foundation after seabed consolidation (k=1×10^{-4} m/s, S_r=0.980, E_s=1.6×10^{8} N/m^2, P_v=0 kPa).

Fig. 5. Distributions of the horizontal soil displacements ((a) u_x and (b) u_y) and the effective normal stresses ((c) σ'_x and (d) σ'_y) around the pile foundation (k=1×10^{-4} m/s, S_r=0.980, E_s=1.6×10^{8} N/m^2, de/R=4.7, P_v=0 kPa).

Fig. 6. Distributions of (a) the vertical effective normal stress and (b) the shear stress

around the located and inserted pile foundation after seabed consolidation (k=1×10^{-4} m/s, S_r=0.980, E_s=1.6×10^8 N/m^2, P_v=0 kPa).

Fig. 7. The vertical distributions of the vertical effective normal stress in front of and below the pile foundation for various inserted depths after seabed consolidation (k=1×10^{-4} m/s, S_r=0.980, E_s=1.6×10^8 N/m^2, P_v=0 kPa).

Fig. 8. The maximum amplitudes of the difference in effective stress ($\Delta\sigma'_{\mathrm{zmax}}$) caused by the inserted pile foundation (de/R=3.3, P_v=0 kPa) against (a) the seabed permeability (with S_r=0.980, E_s=1.6×10^8 N/m^2), (b) saturation degree (with k=1×10^{-4} m/s, E_s=1.6×10^8 N/m^2), and (c) seabed Young's modulus (with k=1×10^{-4} m/s, S_r=0.980).

Fig. 9. External loading (P_v=300 kPa) induced excess pore pressure dissipation and the seepage flow around the pile foundation at (a) t=300 s and (b) t=3000 s (k=1×10^{-5} m/s, S_r=0.975, E_s=0.2×10^8 N/m^2, de/R=3.3).

Fig. 10. Temporal variation of (a) the pore pressure, (b) vertical effective normal stress and (c) vertical soil displacement below the pile foundation (k=1×10^{-5} m/s, S_r=0.975, E_s=0.2×10^8 N/m^2, de/R=3.3).

Fig. 11. Effects of the permeability on the excess pore pressure dissipation (S_r=0.975, E_s=0.2×10^8 N/m^2, P_v=300 kPa, de/R=3.3).

Fig. 12. Effects of the saturation degree on the excess pore pressure dissipation (k=1×10^{-5} m/s, E_s=0.2×10^8 N/m^2, P_v=300 kPa, de/R=3.3).

Fig. 13. Distribution of the effective stress σ'_z under various external loadings after seabed consolidation (k=1×10^{-4} m/s, E_s=1.6×10^8 N/m^2, de/R=3.3).

Fig. 14. Sketch of the Mohr-Column criterion.

Fig. 15. Distributions of (a) stress angle φ' and (b) shear failure zone around the pile foundation after seabed consolidation (k=1×10^{-4} m/s, S_r=0.980, E_s=1.6×10^8 N/m^2, P_v=200 kPa, de/R=3.3).

Fig. 16. Effects of the external loading on the shear failure zone around the pile foundation after seabed consolidation (k=1×10^{-4} m/s, S_r=0.980, E_s=1.6×10^8 N/m^2, de/R=3.3).

Fig. 17. Effects of the inserted depth on the shear failure zone around the pile foundation after seabed consolidation (k=1×10^{-4} m/s, S_r=0.980, E_s=1.6×10^8 N/m^2, P_v=300 kPa).

Fig. 18. Wave-induced pore pressure distribution (a and b) and liquefaction depth (c and d) under a progressive wave at two time instants of t=3/8T (left column) and t=5/8T (right column), respectively.

Fig. 19. Effects of the seabed initial consolidation state on the wave-induced liquefaction depth around a pile foundation (de/R=4).

Fig. 20. The maximum liquefaction zone around a pile foundation for various inserted depths.

Table 1. Parameters used in the case studies

Parameters		Notations	Magnitudes	Units
	Radius	R	1.5	m
	Density	ρ_p	2650	Kg/m^3
Pile foundation	Young's modulus	E_p	2.5	GPa
	Poisson's ratio	μ_p	0.25	-
	Pile length	l	12	m
	Inserted depth	de	0, 3, 5, 7	m
	External loading	P_v	0, 200, 300, 400	kPa
Static water	Depth	d	4	m
	Density	ρ_f	1000	Kg/m^3
	Permeability	k	1×10^{-5}, 5×10^{-5}, 1×10^{-4}	m/s
	Porosity	n	0.3	-
Seabed	Density	ρ_s	2650	Kg/m^3
	Saturation degree	S_r	0.975, 0.980, 0.985	-
	Poisson's ratio	μ_s	0.33	-
	Young's modulus	E_s	0.02, 0.06, 0.16	GPa

Figure 1

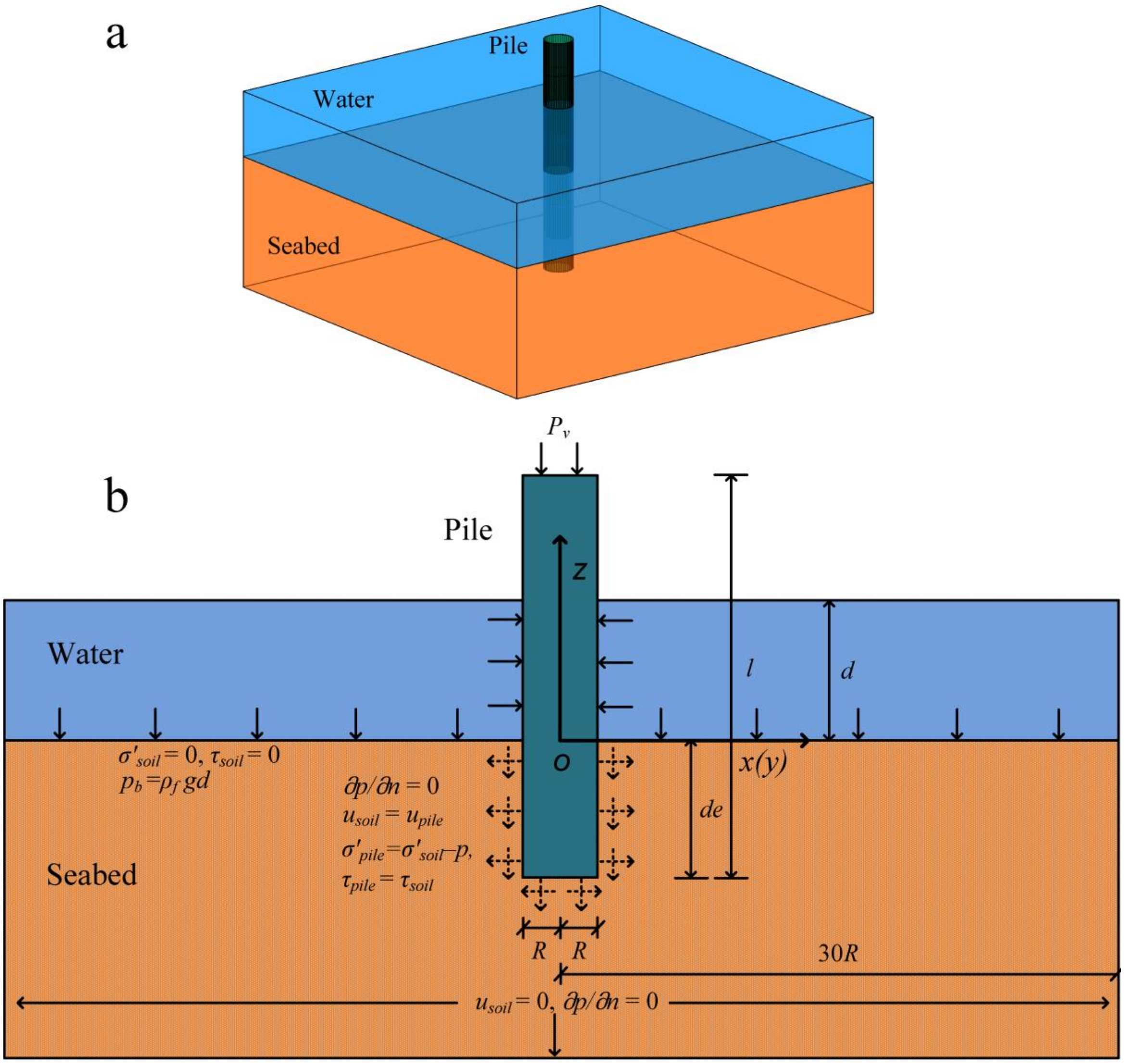
a
Pile
Water
Seabed
b
P_v
Pile
z
Water
l
d
$\sigma'_{soil} = 0$, $\tau_{soil} = 0$
$p_b = \rho_f g d$
o
x(y)
$\partial p/\partial n = 0$
$u_{soil} = u_{pile}$
$\sigma'_{pile} = \sigma'_{soil} - p$,
$\tau_{pile} = \tau_{soil}$
de
Seabed
R
R
30R
$u_{soil} = 0$, $\partial p/\partial n = 0$

Figure 2

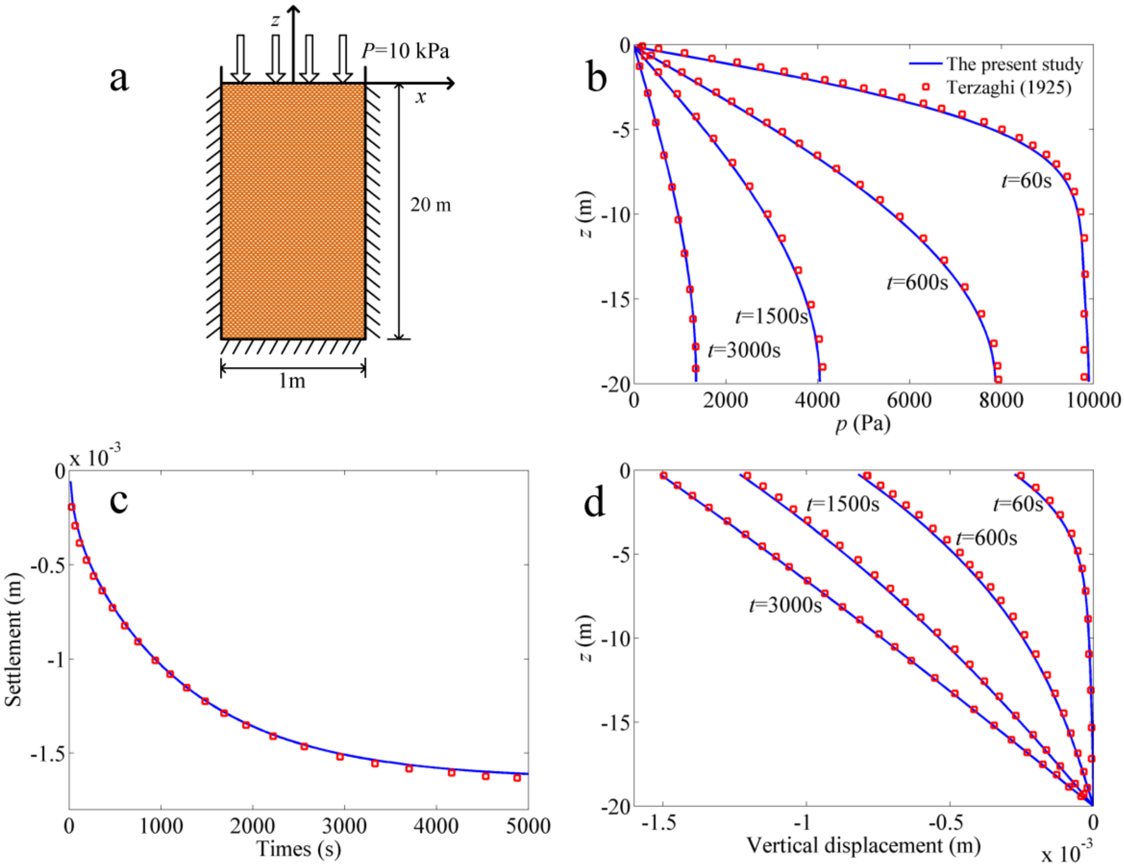
a
z
x
P=10 kPa
20 m
1m
b
The present study
Terzaghi (1925)
t=60s
t=600s
t=1500s
t=3000s
z (m)
p (Pa)
0
-5
-10
-15
-20
0
2000
4000
6000
8000
10000
c
x 10^-3
Settlement (m)
Times (s)
0
-0.5
-1
-1.5
0
1000
2000
3000
4000
5000
d
t=60s
t=600s
t=1500s
t=3000s
z (m)
Vertical displacement (m)
x 10^-3
-1.5
-1
-0.5
0

Figure 3

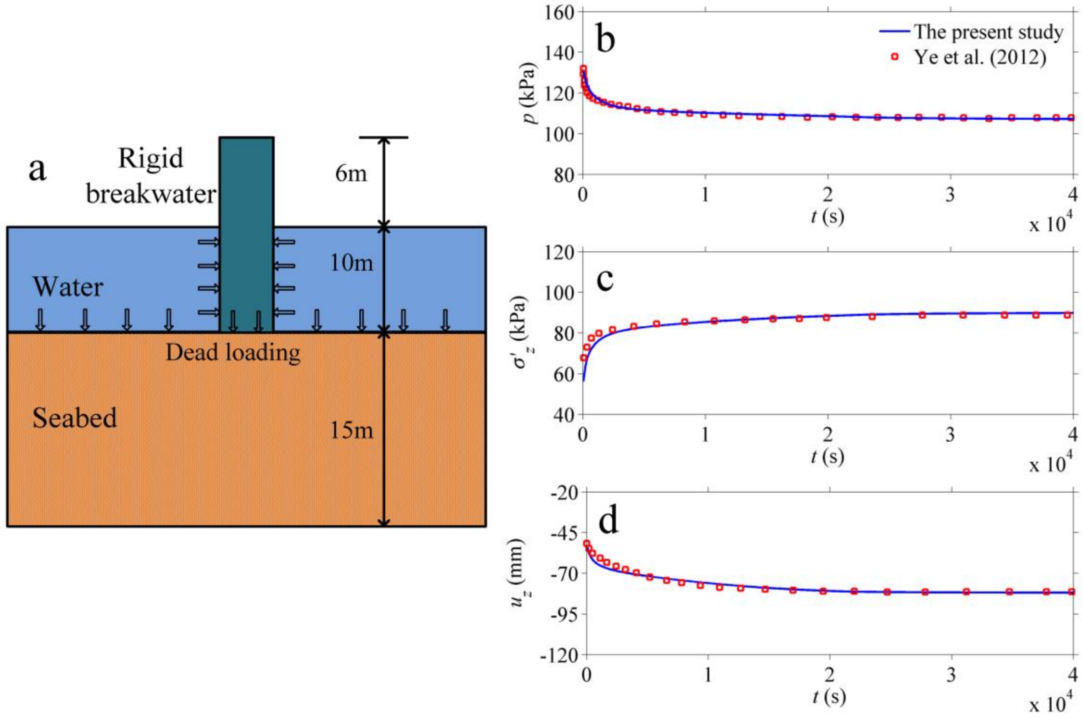
a
Rigid
breakwater
6m
Water
10m
Dead loading
Seabed
15m
b
The present study
Ye et al. (2012)
p (kPa)
t (s)
x 10^4
c
σ'z (kPa)
d
uz (mm)

Figure 4

su

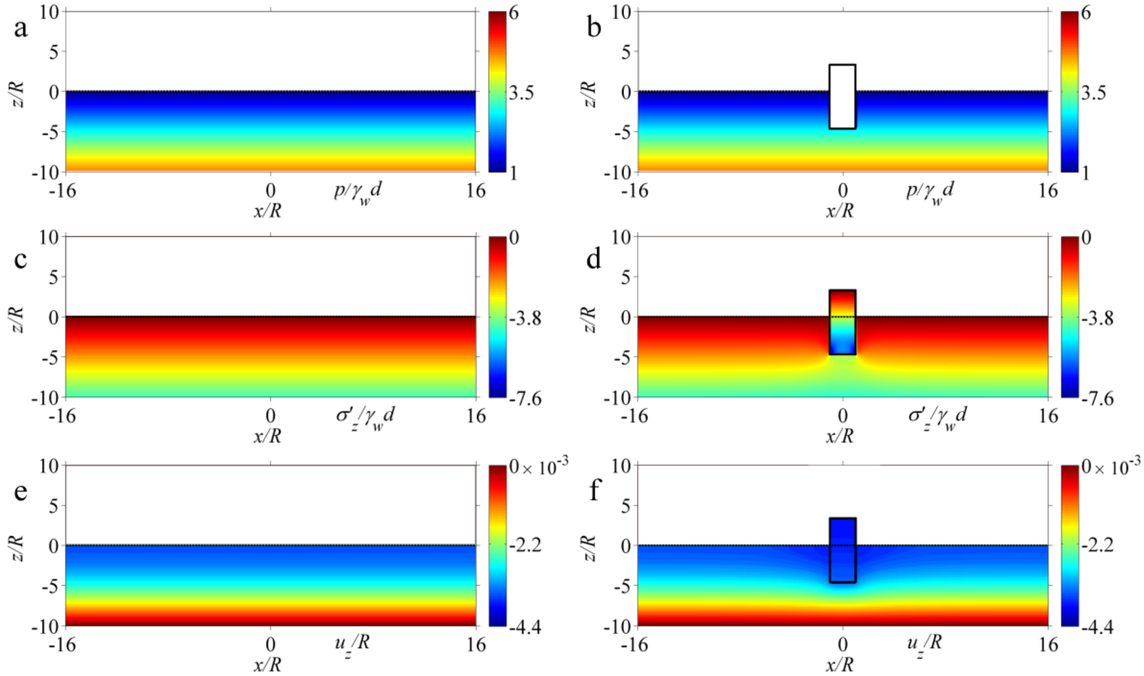
a
b
c
d
e
f
z/R
x/R
p/γ_w d
σ'_z/γ_w d
u_z/R
0 × 10^-3
-16
0
16
10
5
0
-5
-10
6
3.5
1
0
-3.8
-7.6
-2.2
-4.4

Figure 5

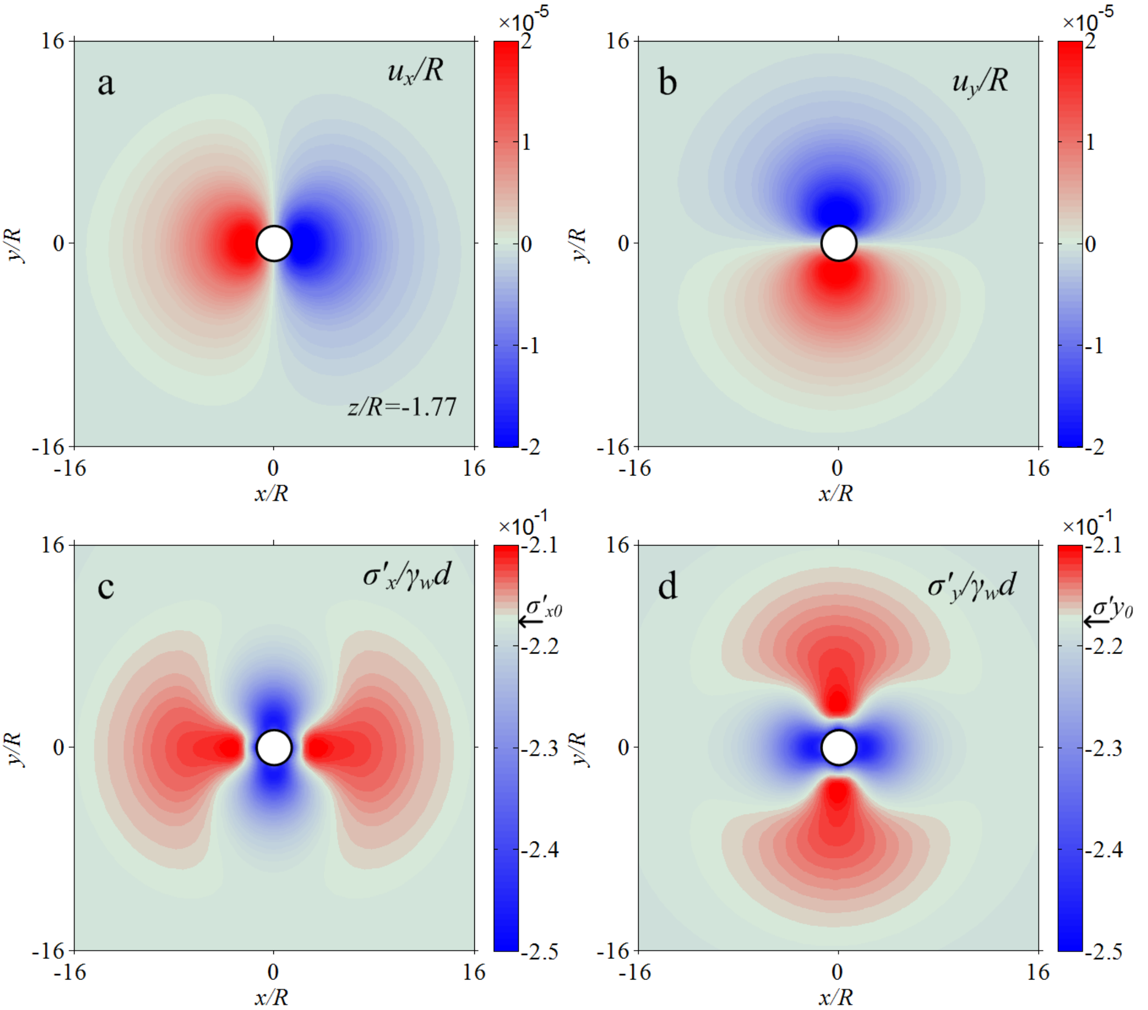
a
u_x/R
z/R=-1.77
b
u_y/R
c
$\sigma'_x/\gamma_w d$
σ'_{x0}
d
$\sigma'_y/\gamma_w d$
σ'_{y0}
$\times 10^{-5}$
$\times 10^{-1}$
x/R
y/R

Figure 6

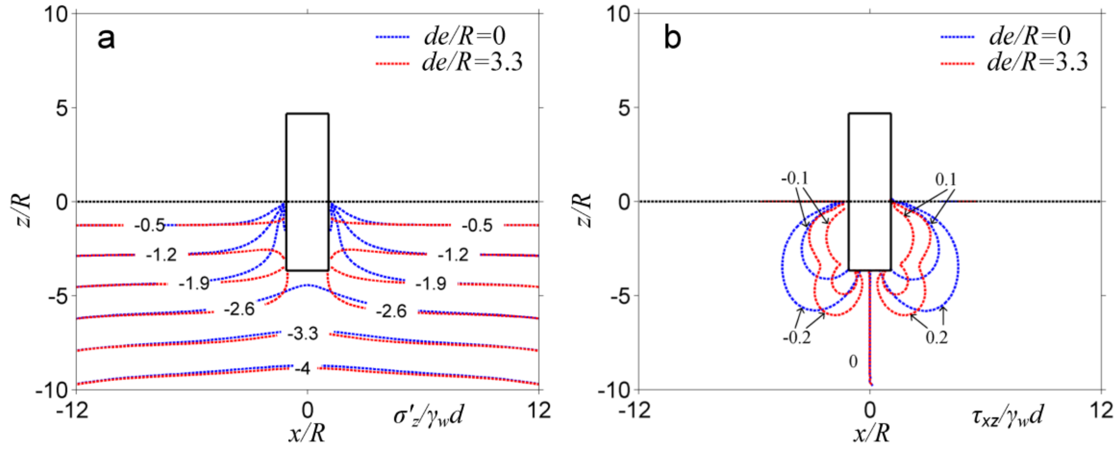

a
de/R=0
de/R=3.3
-0.5
-1.2
-1.9
-2.6
-3.3
-4
z/R
x/R
σ'z/γwd
b
de/R=0
de/R=3.3
-0.1
0.1
-0.2
0.2
0
z/R
x/R
τxz/γwd

Figure 7

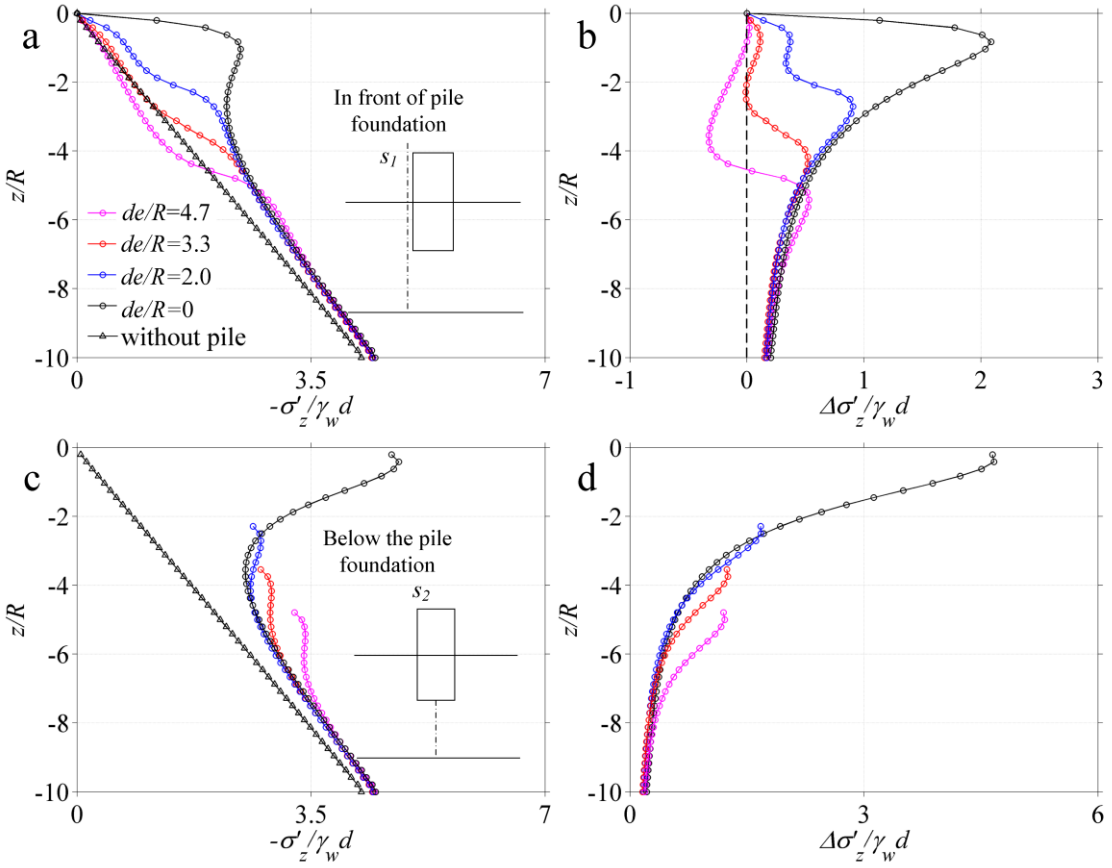
a
b
c
d
In front of pile foundation
Below the pile foundation
s1
s2
de/R=4.7
de/R=3.3
de/R=2.0
de/R=0
without pile
z/R
-σ'z/γwd
Δσ'z/γwd

Figure 8

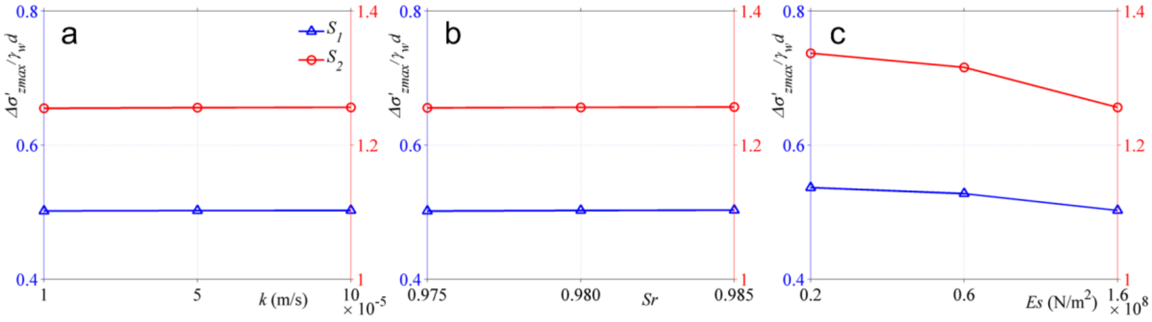
a
b
c
S_1
S_2
$\Delta\sigma'_{zmax}/\gamma_w d$
0.8
0.6
0.4
1.4
1.2
1
k (m/s)
1
5
10
× 10⁻⁵
0.975
0.980
0.985
Sr
0.2
0.6
1.6
Es (N/m²)
× 10⁸

Figure 9

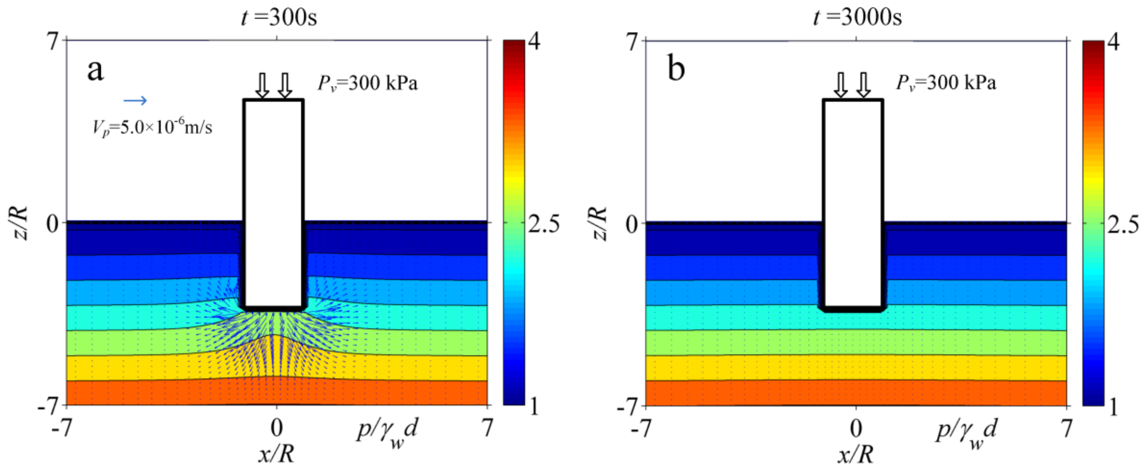
t =300s
a
P_v=300 kPa
V_p=5.0×10^-6m/s
z/R
x/R
p/γ_w d
t =3000s
b
P_v=300 kPa
z/R
x/R
p/γ_w d

Figure 10

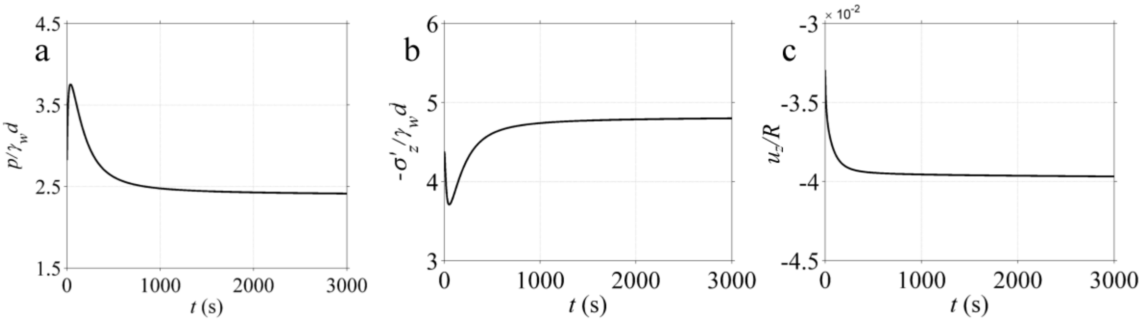

Figure 11

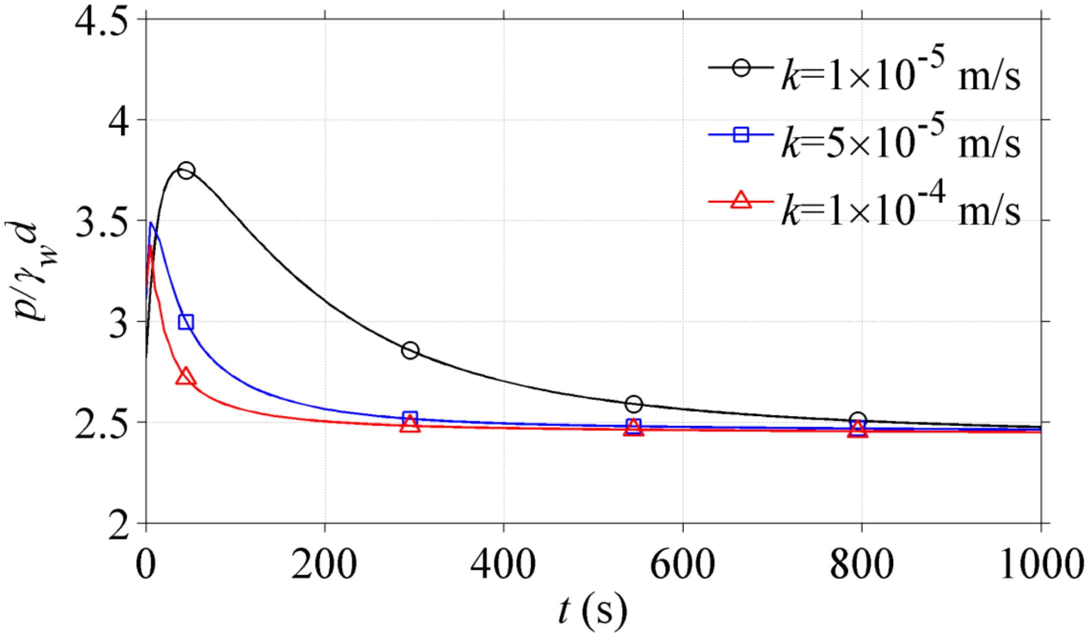

k=1×10^{-5} m/s
k=5×10^{-5} m/s
k=1×10^{-4} m/s
$p/\gamma_w d$
t (s)
4.5
4
3.5
3
2.5
2
0
200
400
600
800
1000

Figure 12

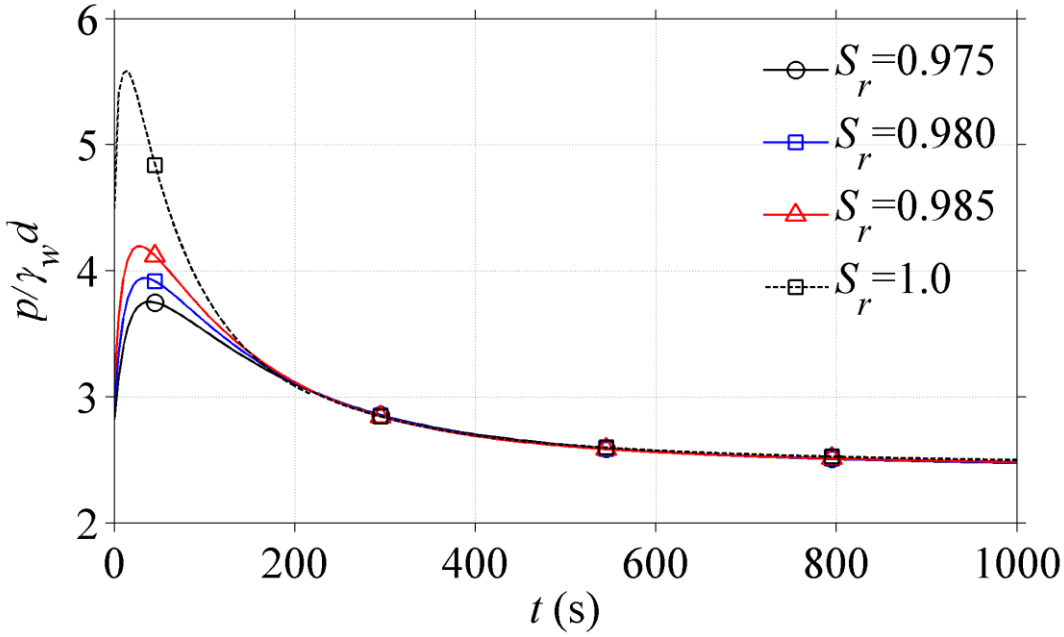

6
5
4
3
2
0
200
400
600
800
1000
$p/\gamma_w d$
t (s)
S_r=0.975
S_r=0.980
S_r=0.985
S_r=1.0

Figure 13

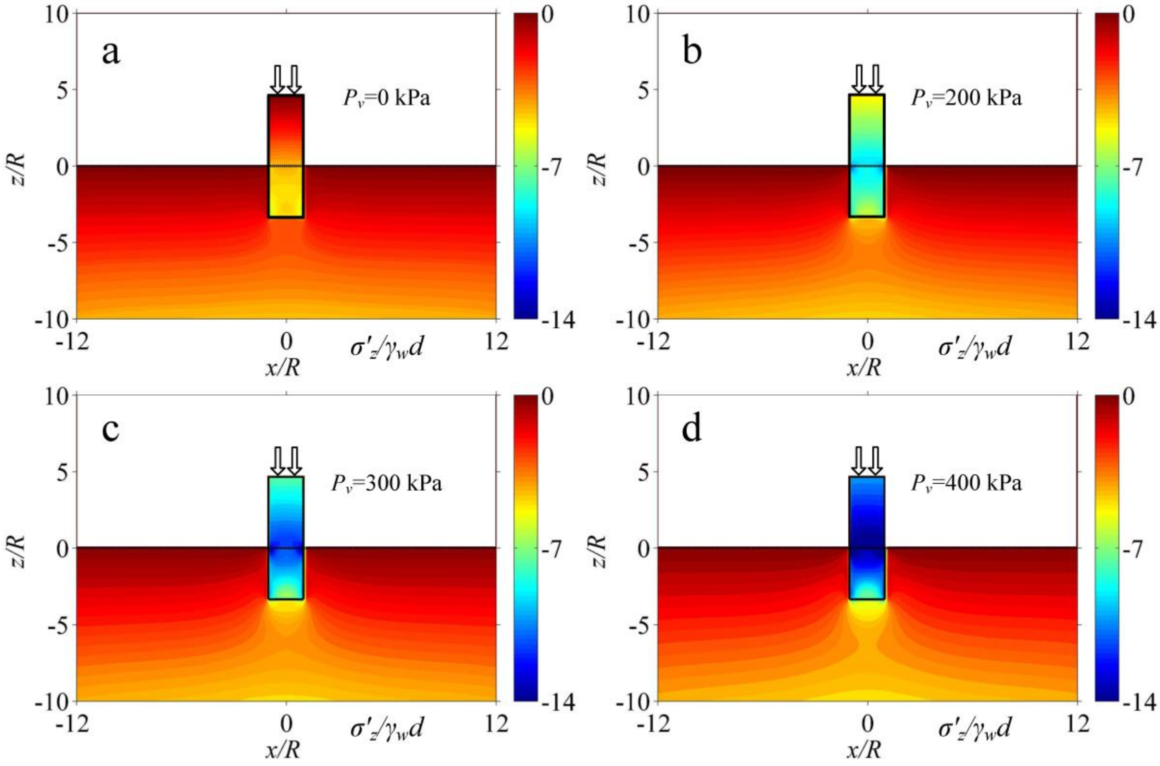

a
P_v=0 kPa
b
P_v=200 kPa
c
P_v=300 kPa
d
P_v=400 kPa
z/R
x/R
$\sigma'_z/\gamma_w d$
0
-7
-14
10
5
0
-5
-10
-12
0
12

Figure 14

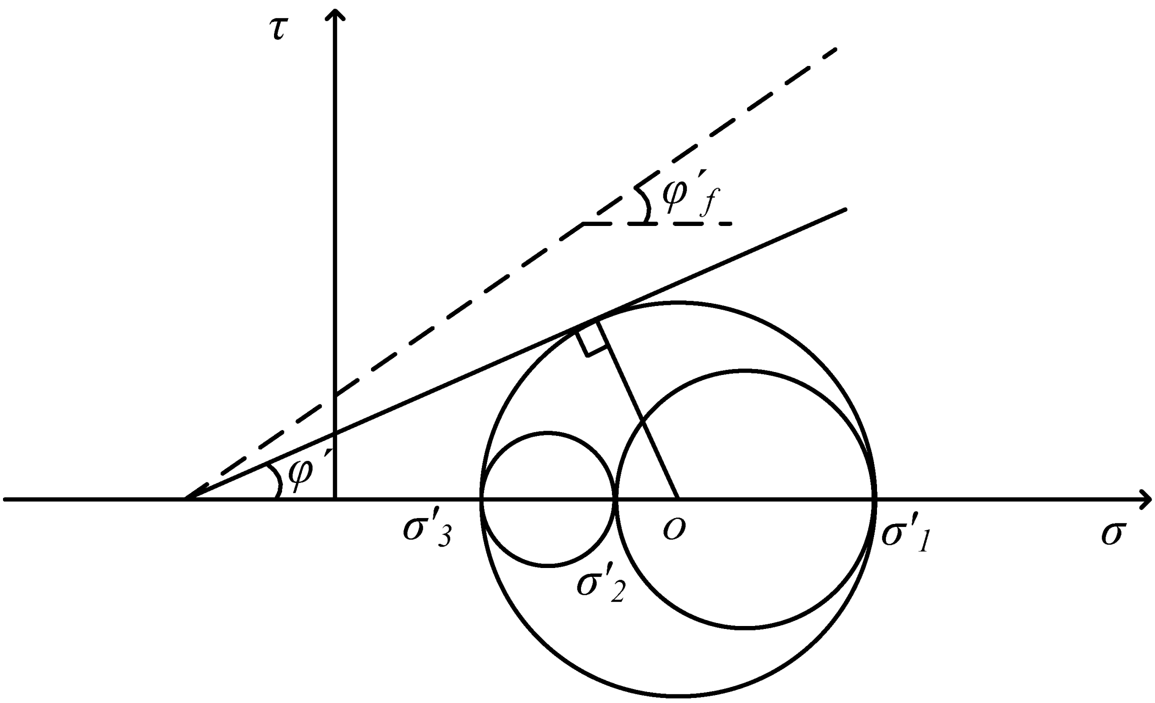

Figure 15

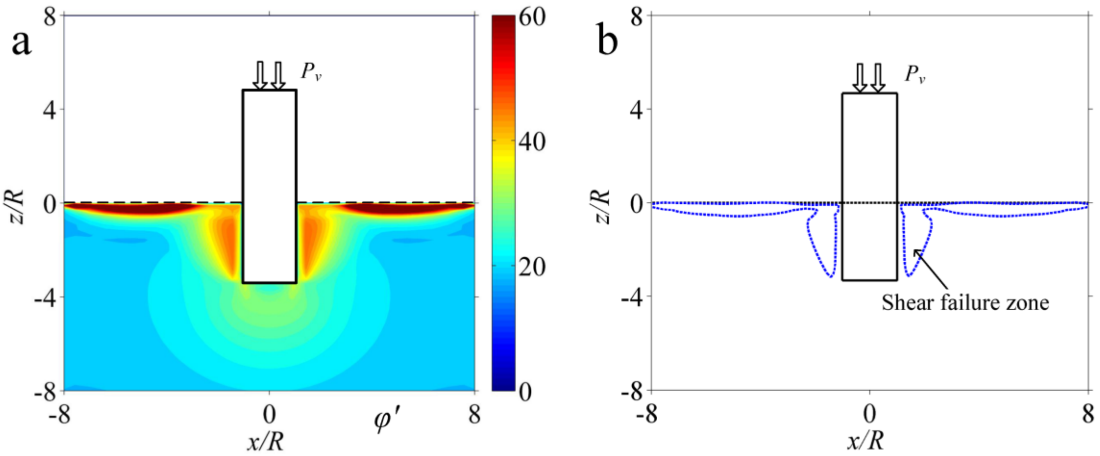

Figure 16

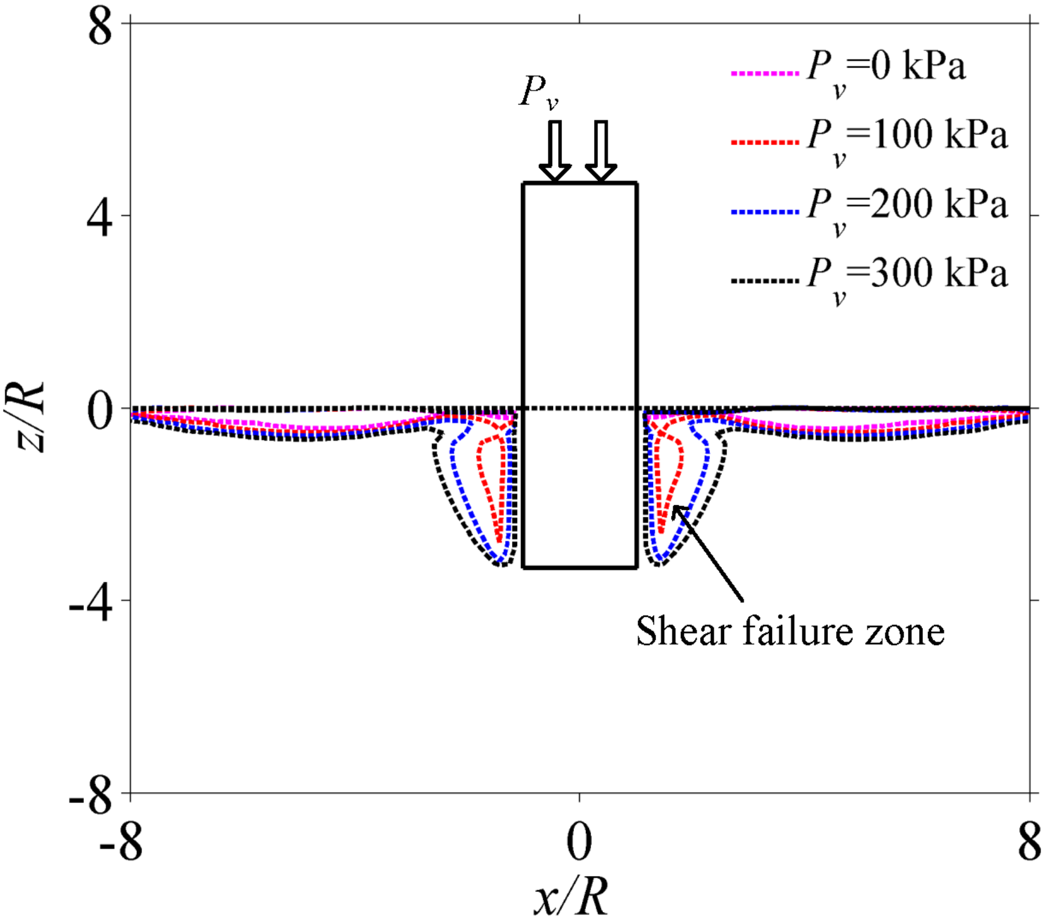
P_v=0 kPa
P_v=100 kPa
P_v=200 kPa
P_v=300 kPa
P_v
Shear failure zone
z/R
x/R
8
4
0
-4
-8
-8
0
8

Figure 17

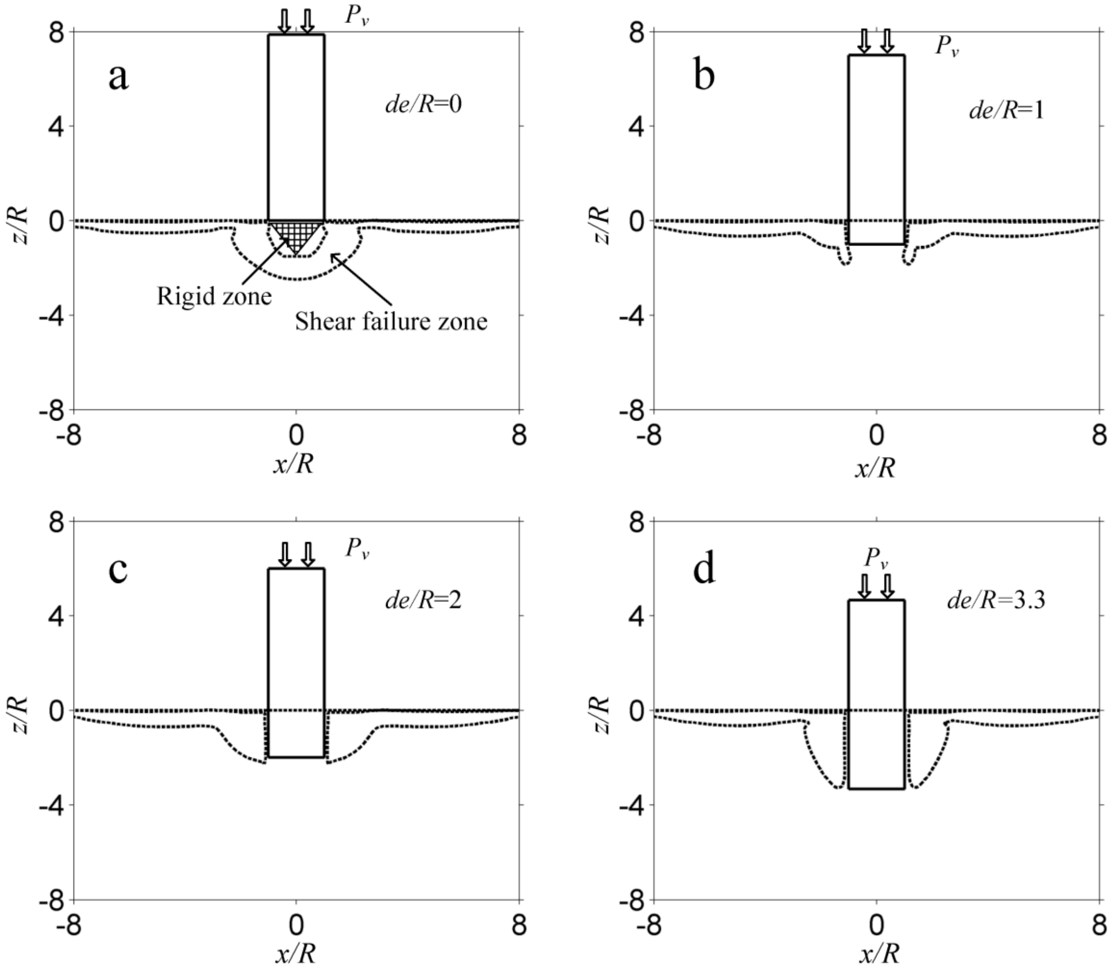
a
P_v
de/R=0
Rigid zone
Shear failure zone
b
P_v
de/R=1
c
P_v
de/R=2
d
P_v
de/R=3.3
z/R
x/R
8
4
0
-4
-8
-8
0
8

Figure 18

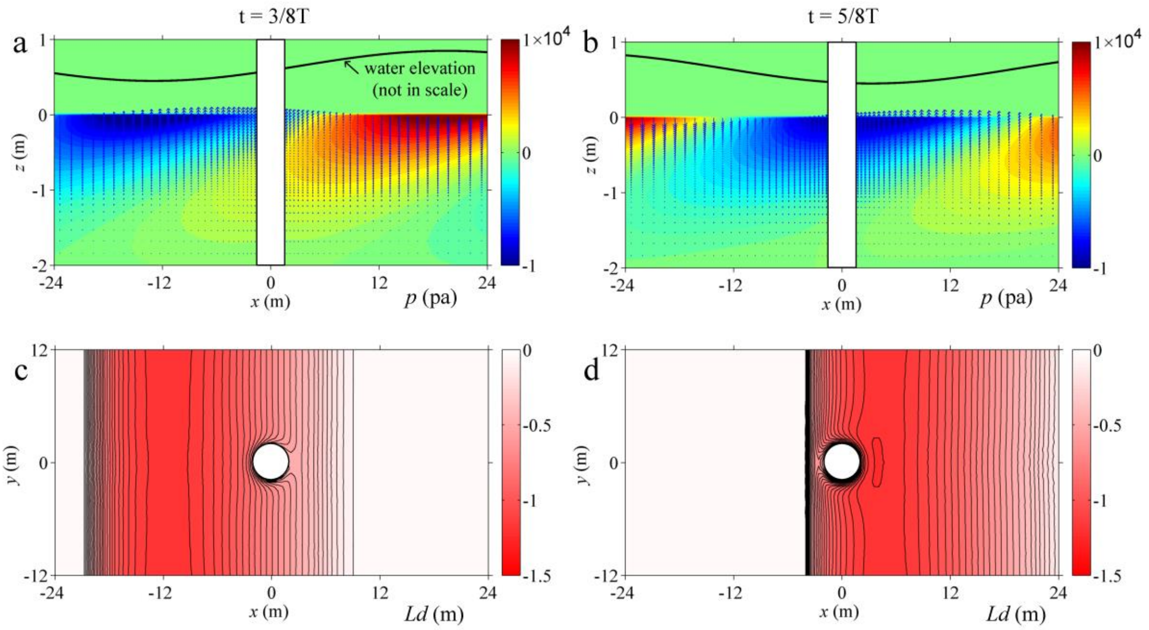
t = 3/8T
t = 5/8T
a
b
c
d
water elevation
(not in scale)
z (m)
y (m)
x (m)
p (pa)
Ld (m)
1×10^4
-24
-12
0
12
24
-0.5
-1
-1.5

Figure 19

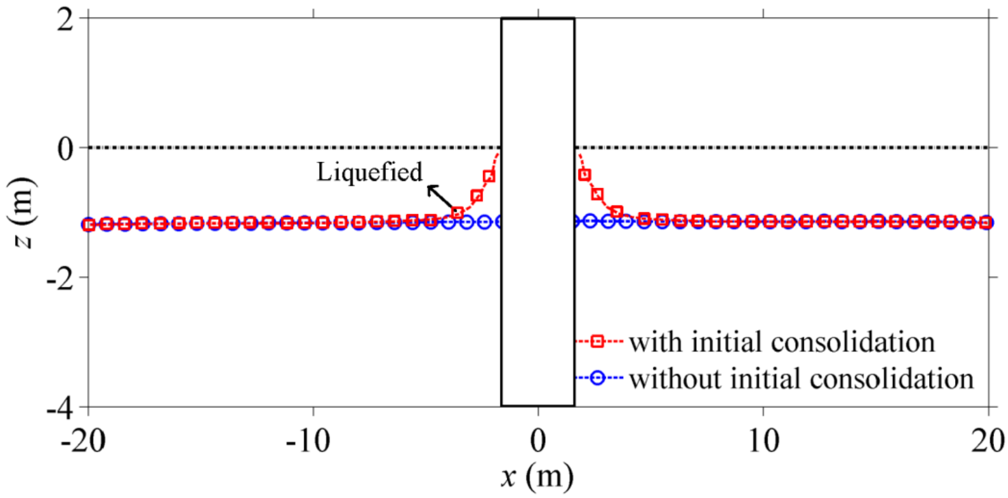

Liquefied
with initial consolidation
without initial consolidation
z (m)
x (m)
2
0
-2
-4
-20
-10
0
10
20

Figure 20